SRC TR 88-89

TECHNICAL RESEARCH REPORT

Optimized Hole Shapes In A Tall Beam

by

A. J. Durelli, S. Azarm and S. Bhandarkar

SYSTEMS RESEARCH CENTER

UNIVERSITY OF MARYLAND

COLLEGE PARK, MARYLAND 20742

OPTIMIZED HOLE SHAPES IN A TALL BEAM

A.J. Durelli, S. Azarm and S. Bhandarkar

Department of Mechanical Engineering
and
Systems Research Center
The University of Maryland
College Park, MD 20742

Abstract

This paper follows a recent paper in Experimental Mechanics, also dealing with optimization. The objectives besides the attempt at optimizations of the design of in-plane loaded tall beams are 1) to discuss the properties of some of the designs obtained; and 2) to compare and evaluate experimental and numerical methods. The optimal hole shape introduced in the beam decreases its weight, has an approximately uniform tangential stress along its boundary and does not increase the maximum tensile stress present originally in the solid beam. The numerical method used is based on finite element analysis and non-linear programming. The experimental method is based on photoelasticity. Emphasis is placed on the results obtained rather than on the description of the methodologies. Practical difficulties, assumptions, accuracy, and the applicability of the two methods are also discussed.

Introduction

Numerous contributions can be found dealing with the analysis of tall beams subjected to in-plane loading. Conway et al.[1] have proposed the superposition of two stress functions and refer to several other approaches. A discussion of the paper was published by Durelli.[2] More references related to the tall beam and in particular concrete walls can also be found in Cardenas et al.[3] In these

papers however, only analyses of the plain solid beams are performed without any attempt to redesign any of them. The optimization process used in the design of the tall beam has been recently addressed by Durelli and Ranganayakamma[4] and Azarm et al.[5] In this paper however, attention is given to the results obtained and to the limitation and applicability of the methods utilized.

The rectangular tall beam is shown in Fig. 1. It is under uniform compressive in-plane loading on the top and is supported at each bottom-end. The optimization approach followed consists of removing material from the beam to decrease its weight. This has been done by cutting a hole (and changing its shape and size) so that it has constant tangential stress along its boundary, buckling is not considered. At the same time, the following constraints have to be satisfied:

1) The ratio of the height H of the beam (Fig. 1) to its width W is 0.75; 2) the top, bottom and sides of the beam remain straight; 3) the load applied to the top is approximately uniform. If holes are introduced, their boundaries should be load free, symmetrical about the vertical axis of the beam and should not cross the bottom or sides of the beam; 4) each of the two uniform supports at the bottom has a length of L=0.10W. Friction at these supports is equivalent to a horizontal force which for the cases analyzed may vary from 5% to 11% of the vertical load depending on the conditions of the surfaces of contact and the rigidity of the beam; 5) the maximum tensile stress in the beam at any stage of the optimization process should not be greater than the one present in the initial solid beam.

The use of the constraint on the maximum tensile stress assumes that the beam will fail under tension.[6] It is also assumed that the maximum tensile

stress in the beam takes place at a free boundary. If this were not the case the same basic methods could be used, but more elaborate computations would be required. It is sufficient to analyze half of the structure when the numerical method is used.

It should be noted that in general the tangential stress changes from tensile to compressive and vice versa as one moves along the holes boundaries and a sharp gradient of stress exists as the stress goes through zero.

Numerical Method

Numerical methods for shape optimization use the combination of two operations. A finite element analysis of the stresses is combined with a numerical optimization algorithm (the 'optimizer'). Numerical shape optimization techniques have been discussed by Haftka and Grandhi[7] in an extensive review of recent literature. The optimizer utilizes the shape sensitivity derivatives obtained using finite differences to iteratively improve the shape of the boundary. The shape sensitivity derivatives provide a quantitative measure of the change in structural response due to a change in shape.

The shape representation used here is similar to the one used by Fleury.[8] The variable hole boundary is represented by a B-spline, whose shape is controlled by the coordinates of ten control points (Fig. 2). The radii r of control points are the shape variables while the angles θ are fixed. Isoparametric eight-node quadrilateral elements are used for the finite element modelling. Mesh regeneration for each new shape is done by using PATRAN[9].

Figure 3 shows a flowchart of the overall methodology. An initial shape (i.e., initial values of the shape variables for the B-spline) is input by the designer at the beginning of the optimization. Successive iterations consist of

applications of finite element analysis, optimization, and modification of the initial shape (or shape variables) until a satisfactory boundary shape is obtained.

The optimizer needs the formulation of constraints and of an objective function. The objective is to find hole shapes with constant tangential stress along the hole boundary, and can be formulated as follows. The tangential stress is sampled in the elements adjacent to the hole boundary, at the two Gaussian integration points closest to the boundary (Fig. 2). Since the tangential stress may change sign as one moves along the hole boundary, the mean tangential stress should be calculated for each 'same sign' portion of the boundary. Let this mean stress be denoted as σ_k^t, k=1,n, where the index k indicates a 'same sign' portion of the boundary, and n is the number of same sign boundaries.

The variance of the stress is then calculated for each 'same sign' portion of the boundary.

$$V_k(X) = \sum_{i=1}^{\ell} (\sigma_i^t - \sigma_k^t)^2 \quad k=1,n \tag{1}$$

where ℓ is the number of sampled Gaussian integration points for that portion of the boundary indicated by index k, and σ_i is the tangential stress at each sampled Gaussian integration point.

The objective function can now be formulated as

$$\text{Minimize } f(X) = \sum_{k=1}^{n} V_k(X) \tag{2}$$

From the formulation, it is seen that as f(X) tends to zero, the tensile stresses and compressive stresses are independently kept constant along the hole

boundary.

The constraint is that the maximum tensile stress in the optimized design must not exceed that in the solid beam. The tensile stresses in the beam are assumed to be maximum somewhere along the hole or the bottom-boundary between the supports. These stresses will be sampled at the finite element nodes along these free boundaries. The constraints can now be written as

$$gj(X) = \sigma^t_{max} - \sigma^t_j \geq 0 \qquad j=1,m1 \tag{3}$$

where σ^t_j is the tangential stress sampled at the m1 finite element node points on the free boundary, and σ^t_{max} is the maximum tensile stress occurring in the initial solid beam without the hole.

Experimental Method

The experimental method depends on observation of photoelastic "isochromatic" fringes at the axes of which the value of $(\sigma_1-\sigma_2)$ is constant, and proportional to the order of the fringe. Since at free boundaries the stress perpendicular to the boundary is zero, the fringe order gives a direct measure of the tangential stress. The designer of an optimized shape therefore only needs to look at the fringes to verify whether the maximum tensile stress constraint is satisfied.

The material used for the model was Homalite 100. The dimensions were 3"x4". The model was placed in a loading frame. The uniform loading at the top was obtained as shown in Fig. 4. The uniformity is only approximate but by Saint Venant's principle the effects of deviations from the uniform loading are negligible at some distance from the top boundary. Details of the photoelastic

methodology has been discussed, for instance, by Durelli[10]. The introduction of optimization techniques and concepts has been addressed by Durelli and Rajaiah[11].

The experimental method consists of systematic removal of material from the low stressed regions. Fig. 5(a), shows the beam in its initial state without the hole. The presence of a zero isochromatic (zero maximum shear) on the vertical axis of the beam suggests that the hole may be started at this point. It should be remembered, however, that even though the maximum shear stress is zero at this point, the individual normal maximum stresses can be high, so that the machining of a circular hole will increase the individual stress (by a factor of two). Actually the maximum stresses at the edge of the small hole are relatively small. The hole is then systematically enlarged by removing material from those parts of the hole boundary that have lower stress than the rest of the hole boundary.

During the optimization process, it is observed in general that as material is removed from the low stress regions of the boundary: 1) The maximum value of stress somewhere else on the boundary decreases; 2) the position of the low stress shifts; 3) the gradient of stress at that point increases.

When this methodology is pursued, each step of the process gives a boundary along which the value of the stress is constant. This means that at each step, a fringe of progressively increasing order is obtained. Each of these shapes can be considered as an optimum in terms of obtaining a uniform stress distribution over most points of the boundary.

Results and Discussion

The solid beam will be analyzed first. The stress constraints will be pointed out and the position at which to start machining the hole will be indicated. This will be followed by the analysis of the various hole shapes at the successive stages in the process of optimization and the comparison and discussion of the results.

Solid Beam

The photoelastic photograph of the right half of the solid beam is shown in Fig. 5a. The fringes shown are those from the light field, with the axis of the dark field fringes superimposed on it. The value of the maximum shear stress corresponding to a fringe is given by the fringe order times a constant:

$$\frac{\tau_{max}}{p} = 0.6566\ n \qquad (4)$$

where p is the uniform loading on the top in psi (or kg/cm^2) and n is the fringe order.

The following points can be noted:

1. The maximum tensile stress occurs just to the left of the support on the bottom boundary and its corresponding fringe-order is 1.5 ($\sigma^t/p = 1.97$).
2. The zero isochromatic occurs at two points on the vertical axis of the beam near the center.

The material removal started at the position of the zero isochromatic. The constraint that the maximum tensile stress in the beam should not increase beyond that in the solid condition, dictates that the fringe-order at the tensile portions of the boundary should not exceed 1.5 ($\sigma^t/p = 1.97$). As mentioned earlier, this is under the assumption that the maximum tensile stress

occurs only on the load free boundaries. The assumption is reasonable with the possible exception of the contact surfaces at the supports which would require a separate analysis.

The τ_{max} contours obtained numerically for the solid beam are shown in Fig. 5b. A horizontal reaction of 11% of the load on the top, is applied at the support. This value was obtained as required for a horizontal direction equilibrium of the photoelastic specimen.

The following points can be noted:

1. The maximum tensile stress (fringe-order 1.5) occurs at the bottom boundary of the beam near the support. This is clearly shown in both analyses.
2. The two zero isochromatics on the vertical axis correspond to very small values of stress on the numerical analysis.
3. At the support and at the top boundary, the values of the numerically obtained fringes are slightly lower than the ones experimentally obtained. The discrepancies can be attributed to slight differences in the values used as frictional forces applied to the experimental model. It should also be mentioned that these forces will change as the hole shape is modified.
4. The relatively large size of the finite elements used.

Optimized Shapes

Figs. 6(a),7(a),8(a), and 9(a) show four optimized hole shapes obtained experimentally with progressively increasing fringe orders coinciding with the boundary of the hole. It can be observed that:

1. In all the figures, the stress along the horizontal boundary of the hole is tensile, while the stress along the lateral boundaries is for the most part compressive.

2. The tensile and compressive stresses are separated by a zero isochromatic which can be easily identified as the only black fringe when using white light instead of monochromatic light. (The other fringes are colored).
3. The fringe-order at the horizontal boundary is 0.5 in Fig. 6(a) and 0.8 in all of the other cases, which is below the 1.5 limit.
4. In Figs. 7(a), 8(a) and 9(a), there is a short region of tensile tangential stress at the top edge of the hole, with fringe orders of 0.4, 0.8, and 1.5, respectively, In Fig. 9(a), therefore, the tensile stress has reached the 1.5 limit.
5. In all the figures, the maximum tangential stress on the bottom edge of the beam to the left of the support shows a fringe order of 1.5. In Fig. 9(a), any attempt to remove more material along the hole boundary increases the tensile stress beyond the 1.5 limits both at the bottom edge of the beam (to the left of the support) and at the top edge of the hole.

Figs. 6(b),7(b),8(b) and 9(b) show the hole shapes obtained using the numerical method when the horizontal reaction at the supports is 5% of the total load applied. These are quite similar to the corresponding experimental figures, except for the expected local variations at the support and top loaded boundary. The following observations are made:

1. Whereas the experimental method permits only removal of material, the numerical method may also add back previously removed material as the hole gradually approaches to the optimum shape.
2. The efficiency of the optimizer decreases as the optimum is approached and several further iterations may be required to converge to an opti-

mum.

3. The B-spline cannot model sharp curvatures. The top part of the hole in Fig. 8(a), for example, will require more control points in the vicinity of the top of the hole for more precise numerical modelling.

Fig. 10(a)-(d) shows the design variables (corresponding to each of the optimum holes shapes of Figs. 6(b) - 9(b) and the side constraints ($x_i^L \leq x_i \leq x_i^U$). These side constraints are an essential part of the numerical optimization process. They ensure that the hole does not converge to the optimum shape closest to the starting point, but rather converges to the optimum hole shape in the region defined by the side constraints. From these plots the designer can verify if the design has been artificially bounded by the side constraints. Note that the design variables may touch the side constraints only at the two extreme ends of the hole. However if the design variables touch the side constraints anywhere in between, then the side constraints may be preventing the hole from changing shape to attain a constant boundary stress distribution. This is avoided by looking at the side constraint plots at the end of each iteration and changing the side constraints, if necessary.

Fig. 11 shows the variation of the stress tangential to the hole boundary with angle θ as obtained experimentally. Figure 12 shows the corresponding results for the numerical hole shapes sampled at 54 node points along the boundary.

Figure 13 shows a plot of the normalized tangential stress as a function of hole size. The tangential stresses are plotted for four points in the beam - three on the hole boundary and one on the bottom boundary of the beam to the left of the support. Note that the tangential stress at b is compressive, the

stress constraint is not violated even though the curve for b crosses the critical stress curve d.

Conclusion

Some of the general conclusions made are listed below. They include the differences and limitations of the two methods which are important in determining their applicability and accuracy.

1. The accuracy of the stress distributions and the accuracy of the solution depends to a large extent on the correct simulation of the boundary conditions (displacements and forces) that actually occur in the physical structure and are frequently largely unknown. The photoelasticity method is more suitable in this respect, as it can often simulate these boundary conditions closely. Of importance are the frictional forces which occur on the top loaded surface and at the supports. The magnitude of these frictional forces may change as the shape of the hole boundary is varied. Also they are often non-linear in nature for large deflections. Modelling these boundary conditions in the numerical method is in general more difficult than in the experimental method.
2. In general, photoelasticity is faster and less expensive when used on problems that require knowledge of the stress field only on the free boundaries. If structural response in the form of individual stresses is required in the interior of the structure then the numerical method may be faster and less expensive.
3. In regions with high stress gradients, the photoelasticity method is usually more reliable for optimizing the geometry as it gives a more accurate picture of the stress distribution than the one obtained when

the finite element method is used. It should be noted that the regions of high stress gradients keep moving around the boundary as the hole shape is modified. To handle this problem in the numerical method, an adaptive mesh generation can be used, in which, the mesh is refined for each shape in the regions of high stress concentrations, thereby increasing the accuracy of the stress distribution. In general, a robust algorithm is needed for this purpose.

4. The numerical representation of the hole boundary by a B-spline cannot handle some of the possible hole shapes, unless the number of control points is increased (at the cost of increased computer time).
5. Though four 'optimum' hole shapes have been obtained by the two methods, there is no guarantee that even the last of these holes represents the maximum saving in weight (global optimum) for the given constraints. It is possible that other hole shapes with a more complicated geometry than the simple triangular hole may yield a higher saving in weight. Also if the constraints were to be modified to allow multiple discontinuities and removal of material from the load free edges of the beam, then it is reasonable to expect designs which are more effective. The experimental method is better for handling multiple discontinuities than the numerical method, since maintaining mesh integrity and the development of robust mesh generators is difficult in the latter case when multiple discontinuities are present.
6. The numerical method was found to be quite expensive in terms of computer time. However, the design converges to a near optimum shape in four or five iterations, (except the last shape) before the optimizer becomes

inefficient. To cut down on computer time, interaction can be used to manually change the shape after the first few iterations of the optimizer.

7. The four hole shapes obtained are among a family of hole shapes that have an area of approximately uniform stress distribution along the boundary, each with a different value of tangential stress.
8. It should be obvious following this presentation that finite-element methods as well as photoelasticity attempt to obtain the same information and that differences in results are mainly due to different levels of precision, which depend on particular circumstances.
9. Finally, although described here in relation to tall beams, the optimal design method of shapes can be easily applied to a wide variety of structures for weight minimization problems and for minimization of stress concentrations.

References

1. Conway, H.D., Chow, L., and Morgan, G.W., "Analysis of Deep Beams", ASME Journal of Applied Mechanics, Vol. 18, No. 2, pp. 163-172, (1951).

2. Durelli, A.J., "Discussion of Deep Beams", ASME Journal of Applied Mechanics, Vol. 18, No. 4, pp. 421-422, (1951).

3. Cardenas, A.E., Hanson, J.M., Corley, W.G., and Hognestad, E., "Design Provisions for Shear Walls", Proceedings, Journal of the American Concrete Institute, Vol. 70, No. 3, pp. 221-230, (1973).

4. Durelli, A., Ranganayakamma, B., "Optimization Process in Tall Beams", Experimental Mechanics, pp. 259-265 (1988).

5. Azarm, S., Bhandarkar, S., Durelli, A., "On the Experimental vs. Numerical Shape Optimization of a Hole in a Tall Beam", Advances in Design Automation, ASME Publication No. DE- Vol. 14 (S.S. Roo Eds.), pp. 257-264 (1988).

6. Juvinall, R.C., "Engineering Considerations of Stress, Strain and Strength", McGraw-Hill, New York, (1967).

7. Haftka, R.T., and Grandhi, R.V., "Structural Shape Optimization - a Survey", Computer Methods in Applied Mechanics and Engineering, Vol. 57, pp. 91-106, (1986).

8. Fleury, C., "Computer Aided Optimal Design of Elastic Structures", Computer Aided Optimal Design: Structural and Mechanical Systems, C.A. Mota Soares, ed., Springer Verlag, Berlin, pp. 831-900, (1987).

9. PDA Engineering, "PATRAN-G User's Guide", Vol. I & II, (1984).

10. Durelli, A.J. and Riley, W.F., Introduction to Photomechanics, Prentice-Hall, (1965).

11. Durelli, A.J. and Rajaiah, K., "Lighter and Stronger", Experimental Mechanics, Vol. 20, No. 11, pp. 369-380, (1980).

Acknowledgments

The results reported in this paper are in part based on the thesis prepared by S. Bhandarkar to obtain his Master's Degree in Mechanical Engineering at the University of Maryland in College Park.

The methods used are developments in the work conducted by A.J. Durelli on optimization using photoelasticity, and S. Azarm on optimization using numerical methods. They also follow previous efforts by these authors to develop criteria about which one of experimental and numerical methods is more efficient, depending on circumstances. This work was supported in part by NSF Engineering Research Centers Program NSFD-CDR-88003012.

K. Shields and V. Anaele were in charge of the reproduction of the manuscript.

Fig. 1. Geometry and loading of the solid beam to be optimized.

Fig. 2. Finite element mesh model for the right half beam with the hole boundary modelled with ten control points.

Fig. 3. Flow-chart of the numerical shape optimization process.

Fig. 4. Approximation to the uniform loading of the tall beam.

Fig. 5. Photoelastic fringes (a) and numerical contours (b) of the maximum shear stresses for the right-half solid beam.

Fig. 6. Photoelastic fringes (a) and numerical contours (b) for the first stage in the process of optimization.

Fig. 7. Photoelastic fringes (a) and numerical contours (b) for the second stage in the process of optimization.

Fig. 8. Photoelastic fringes (a) and numerical contours (b) for the third stage in the process of optimization.

Fig. 9. Photoelastic fringes (a) and numerical contours (b) for the fourth and last stage in the process of optimization.

Fig. 10. Plots of design variables and side constraints for the numerical method, corresponding to the hole shapes of figs. 6(b)-9(b).

Fig. 11. Variation of the stress tangential to the hole boundary with angle θ for the experimental hole shapes of figs. 6(a) - 9(a)

Fig. 12. Variation of the stress tangential to the hole boundary with angle θ for the numerical hole shapes of figs. 6(b) - 9(b).

Fig. 13. Savings in weight corresponding to four steps of optimization and change in stresses at selected points.

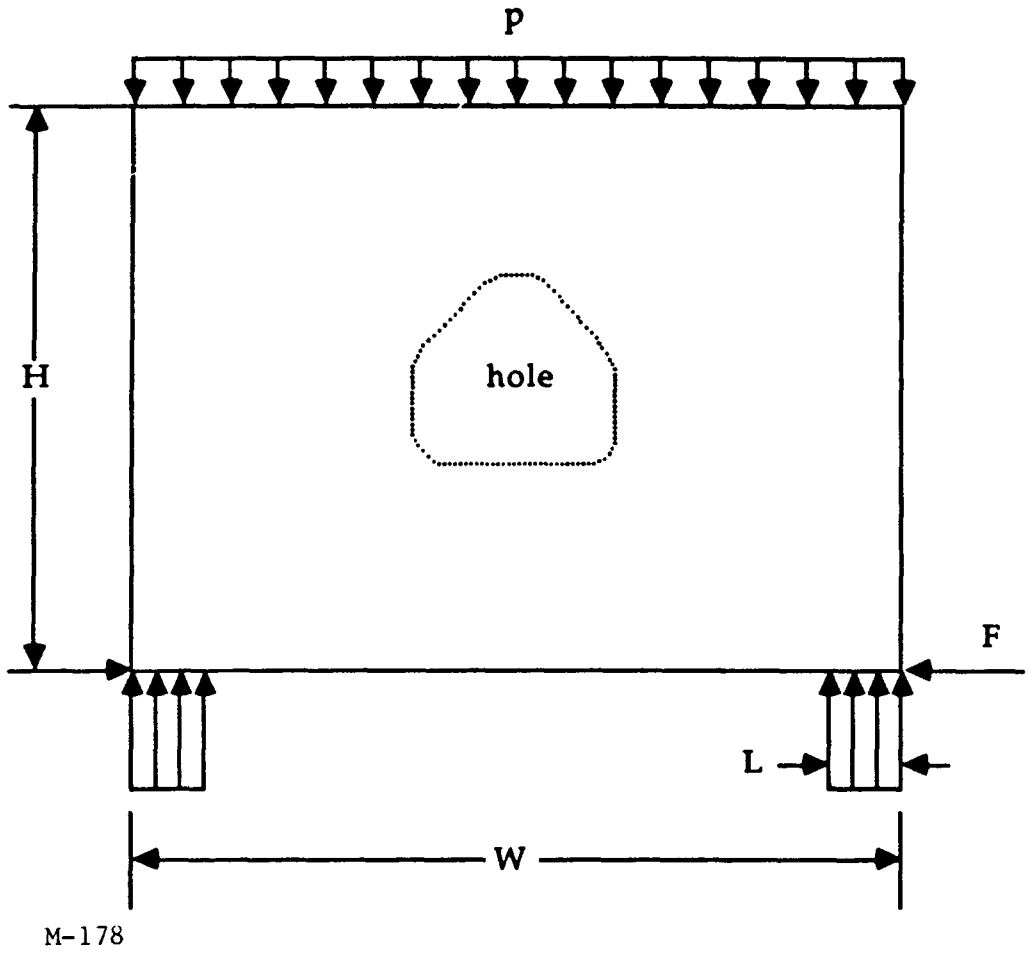

H/W = 0.75

L = 0.1 W

F : Friction

Fig. 1. Geometry and loading of the solid beam to be optimized.

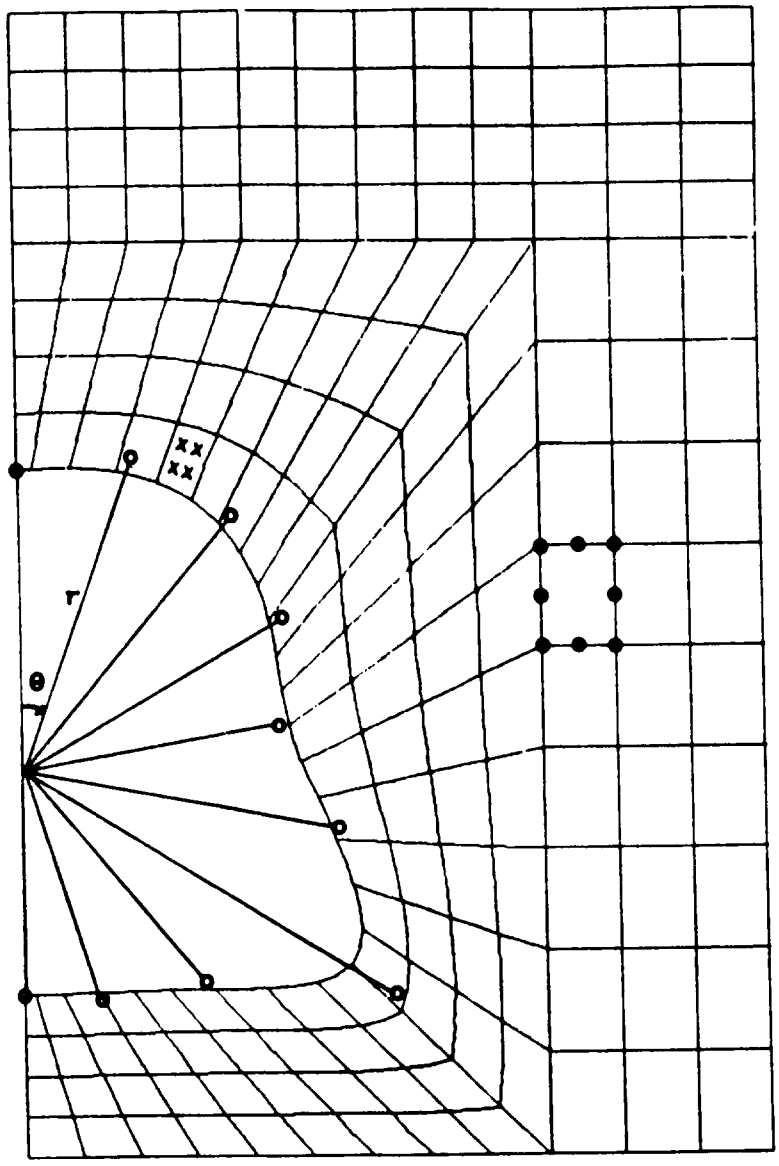

M-179

- o control points
- • finite element nodes
- x 2 x 2 Gaussian integration points

Fig. 2. Finite element mesh model for the right half beam with the hole boundary modelled with ten control points.

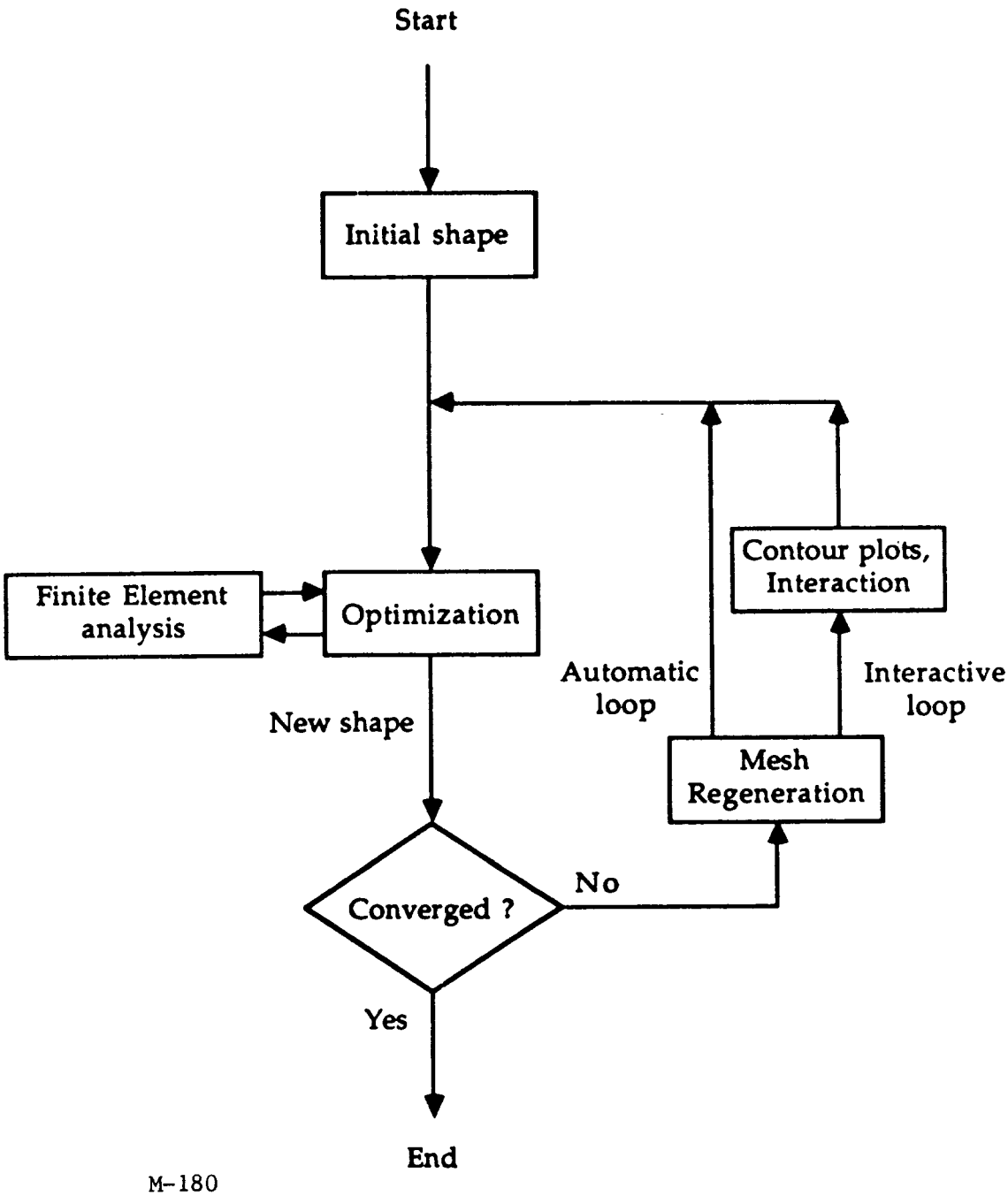

Fig. 3. Flow-chart of the numerical shape optimization process.

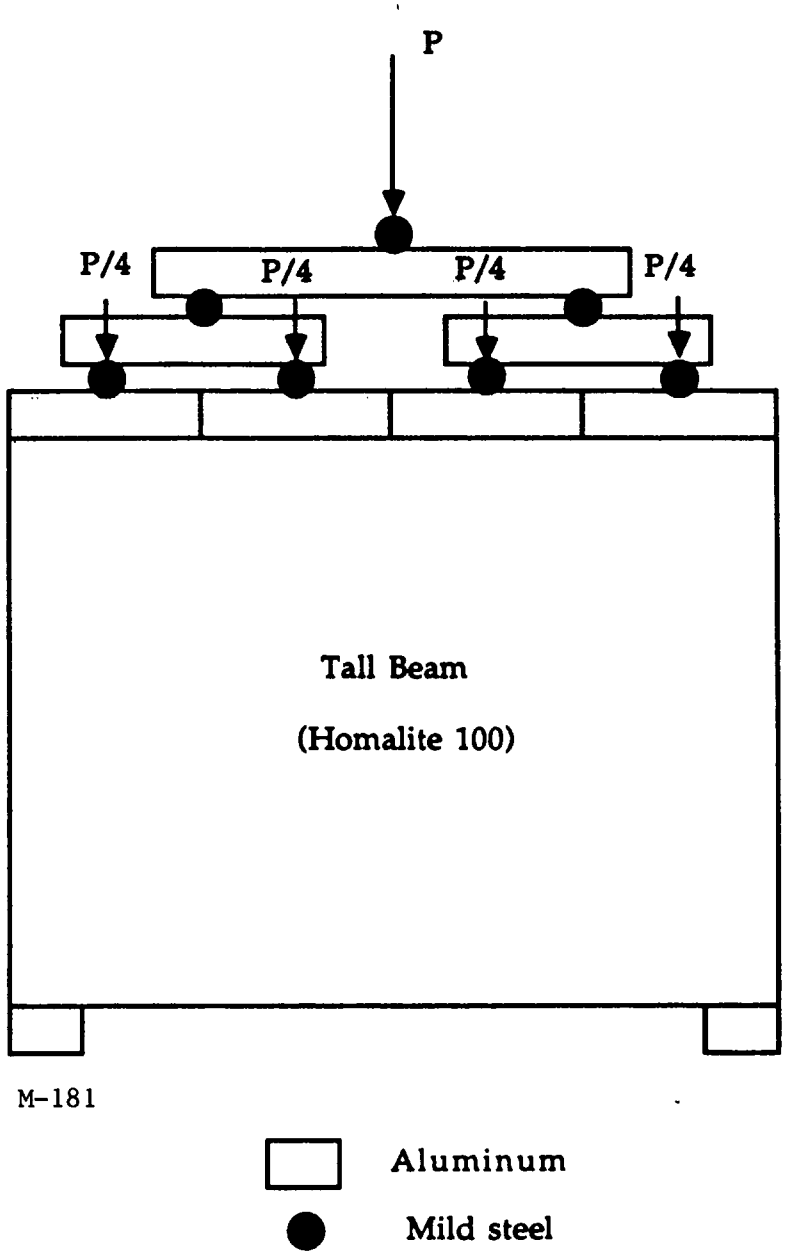

Fig. 4. Approximation to the uniform loading of the tall beam.

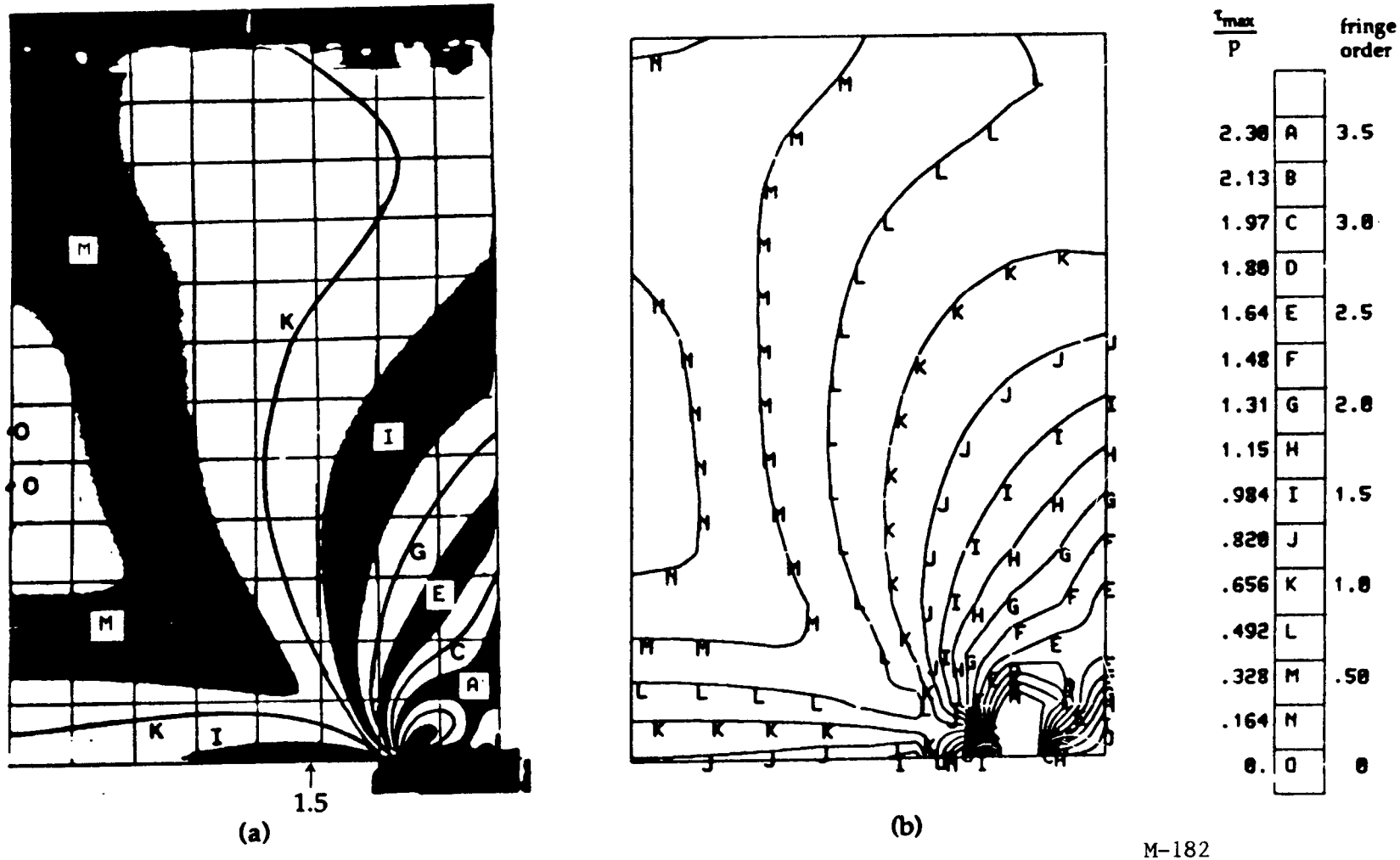

Fig. 5. Photoelastic fringes (a) and numerical contours (b) of the maximum shear stresses for the right-half solid beam.

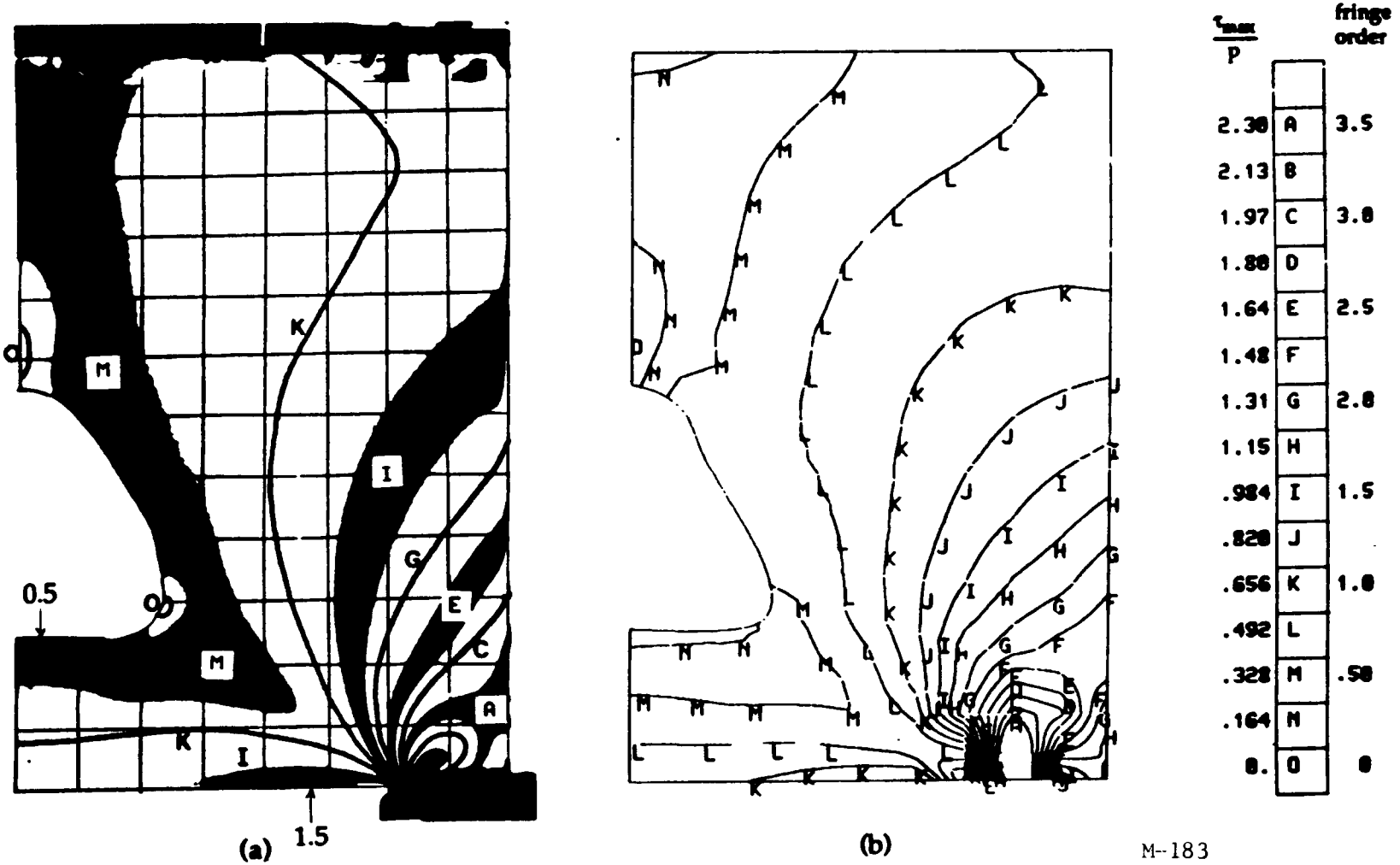

Fig. 6. Photoelastic fringes (a) and numerical contours (b) for the first stage in the process of optimization.

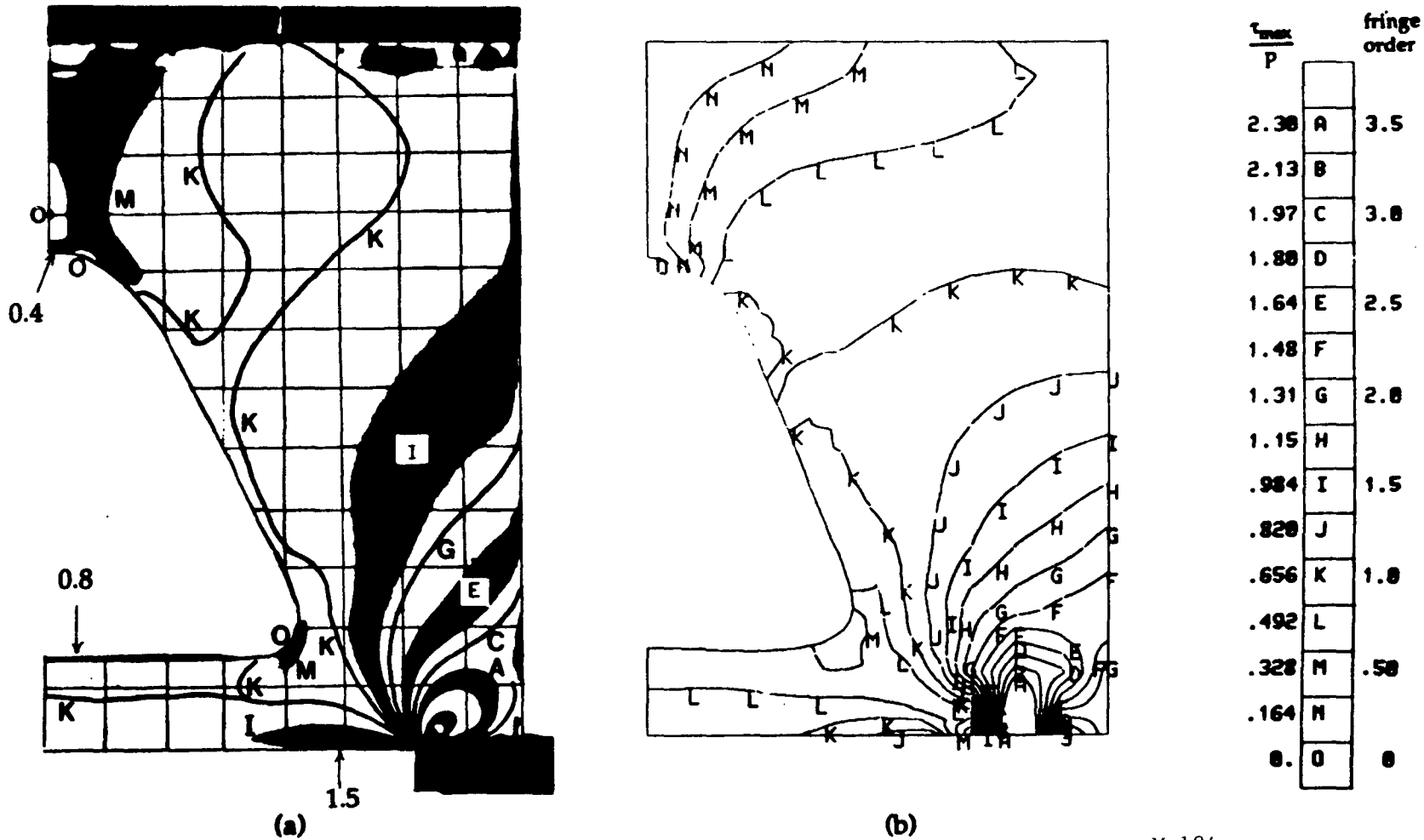

M-184

Fig. 7. Photoelastic fringes (a) and numerical contours (b) for the second stage in the process of optimization.

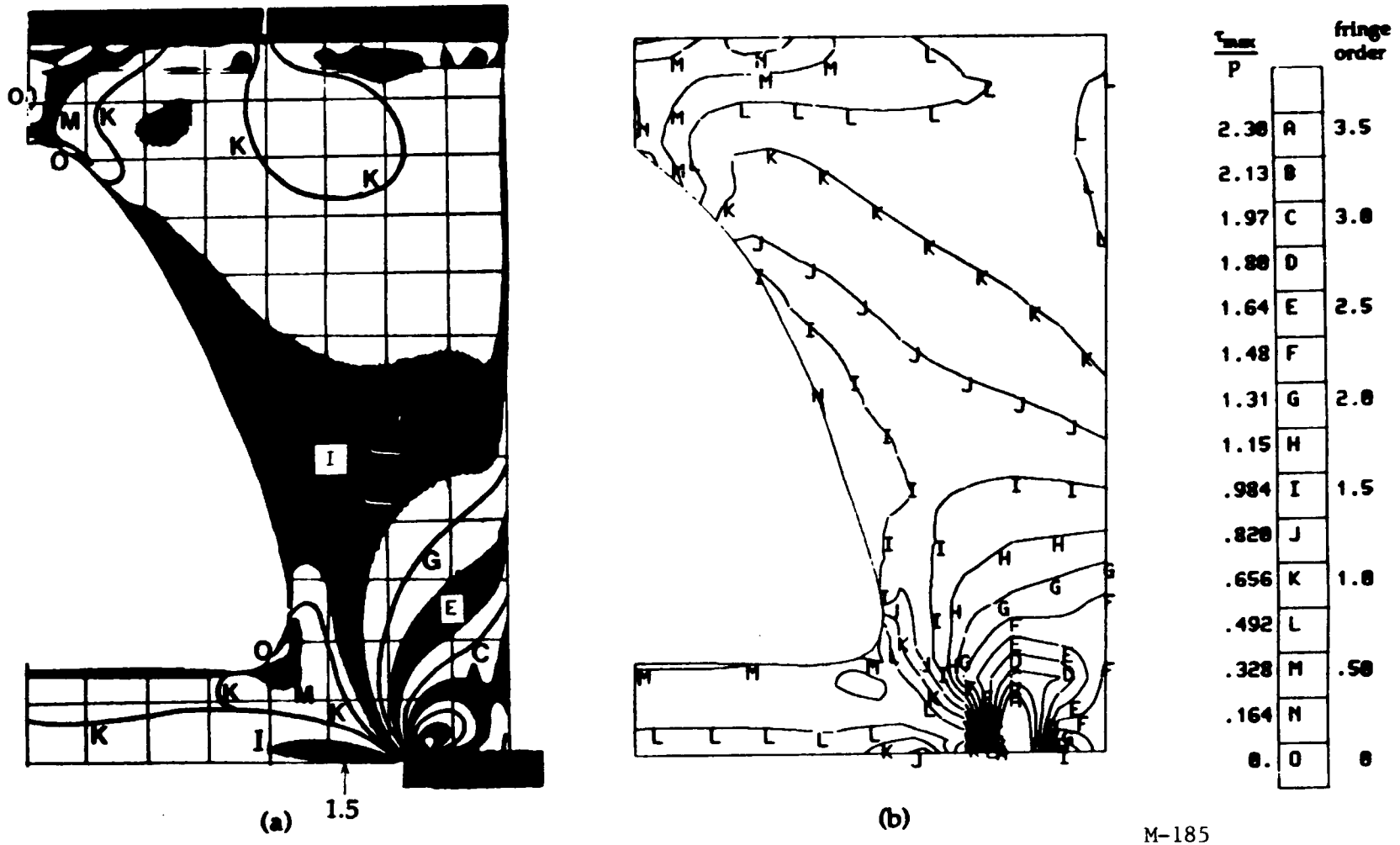

Fig. 8. Photoelastic fringes (a) and numerical contours (b) for the third stage in the process of optimization.

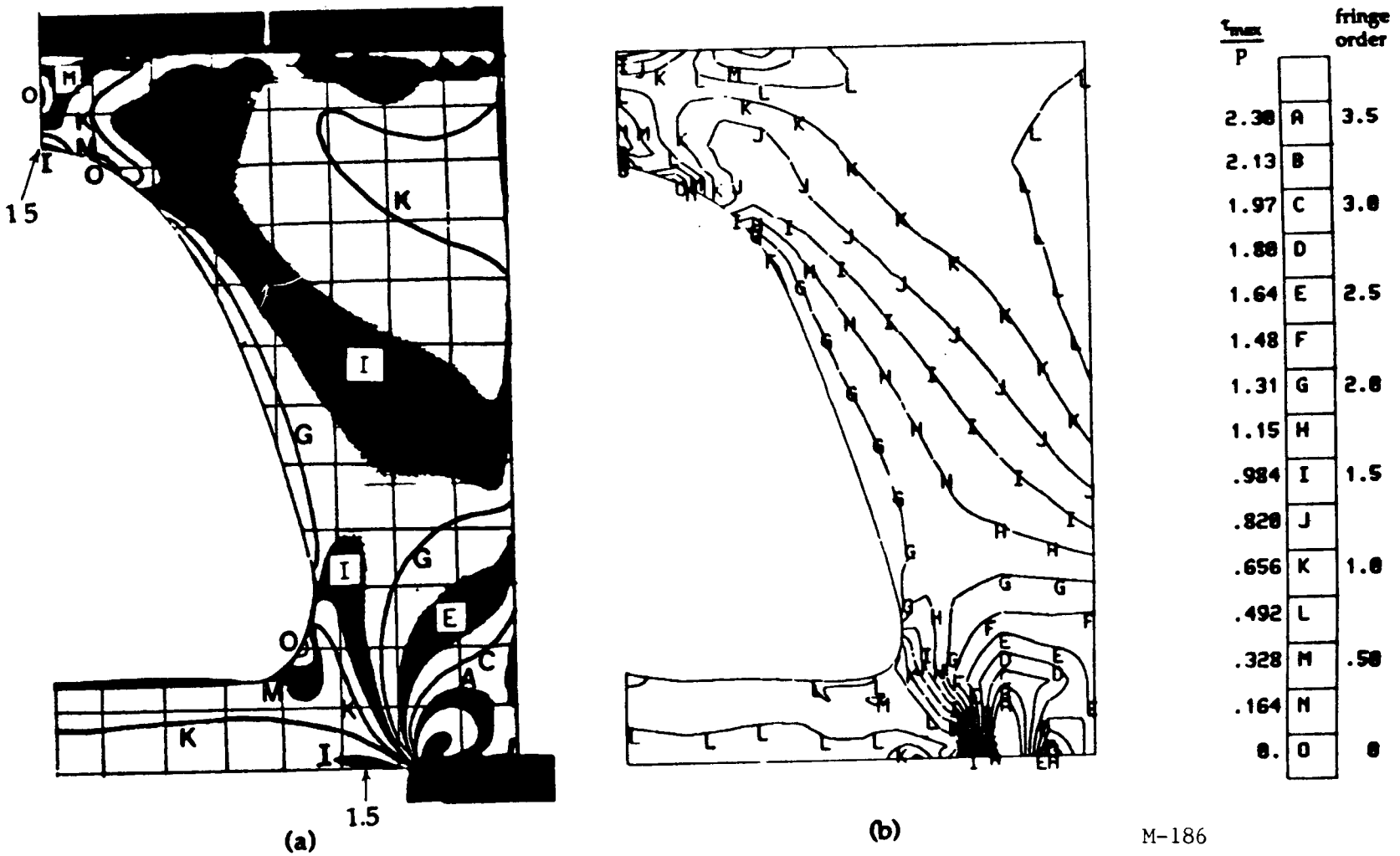

Fig. 9. Photoelastic fringes (a) and numerical contours (b) for the fourth and last stage in the process of optimization.

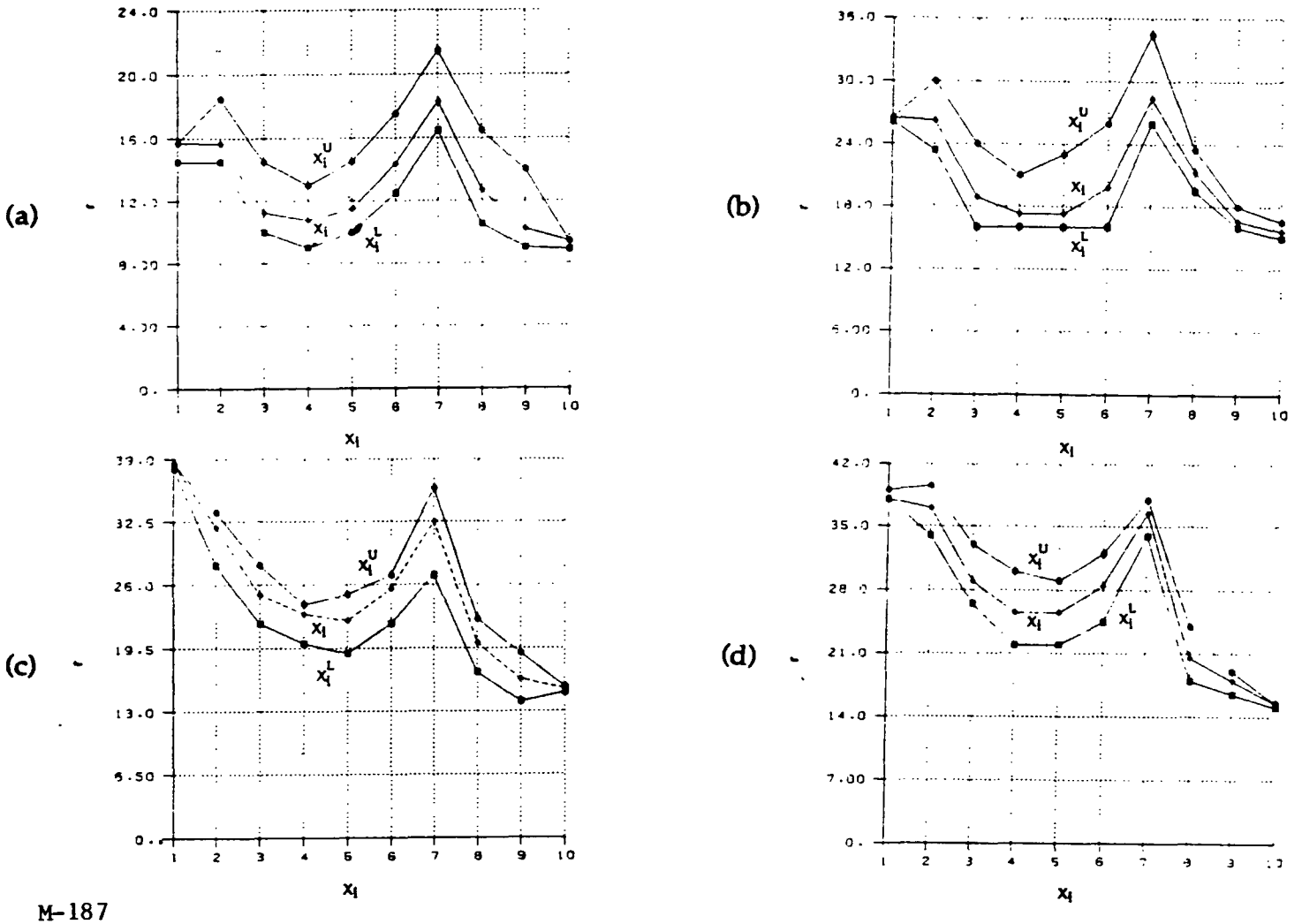

Fig. 10. Plots of design variables and side constraints for the numerical method, corresponding to the hole shapes of figs. 6(b)-9(b).

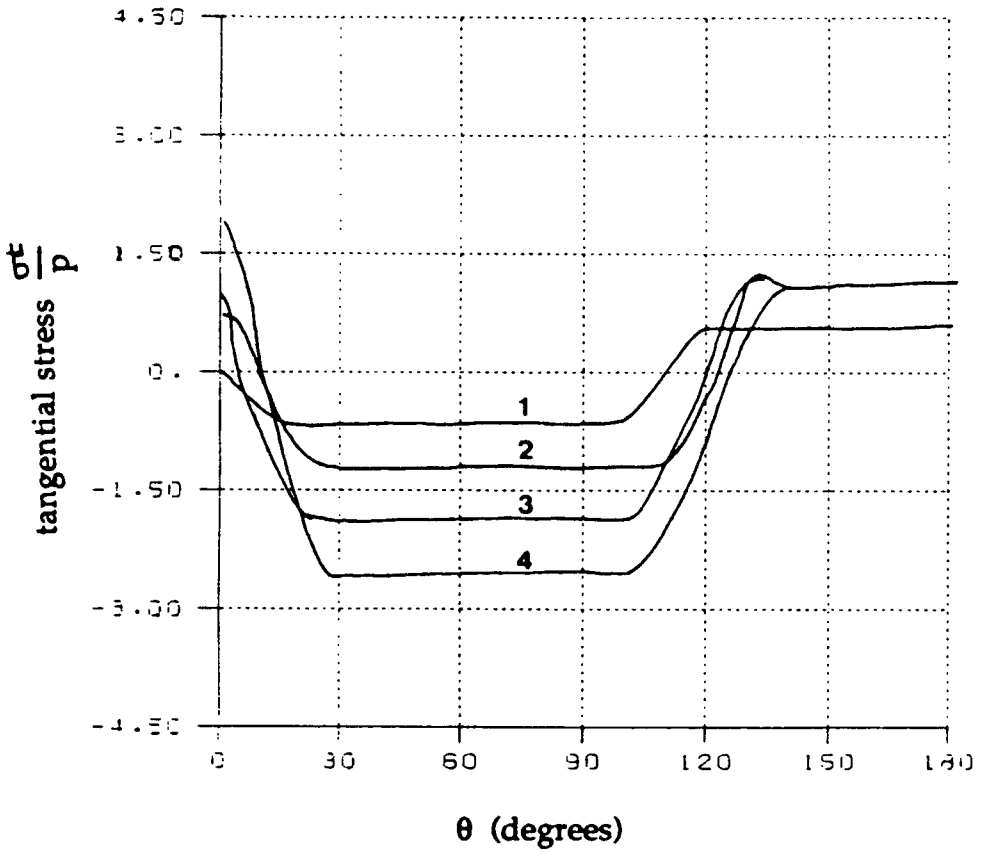

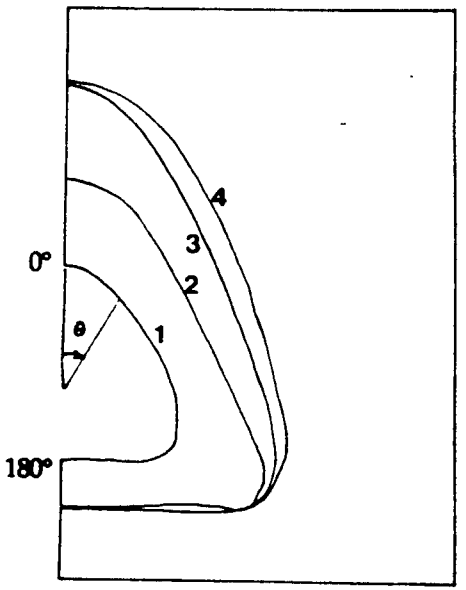

M-188

Fig. 11. Variation of the stress tangential to the hole boundary with angle θ for the experimental hole shapes of figs. 6(a) - 9(a)

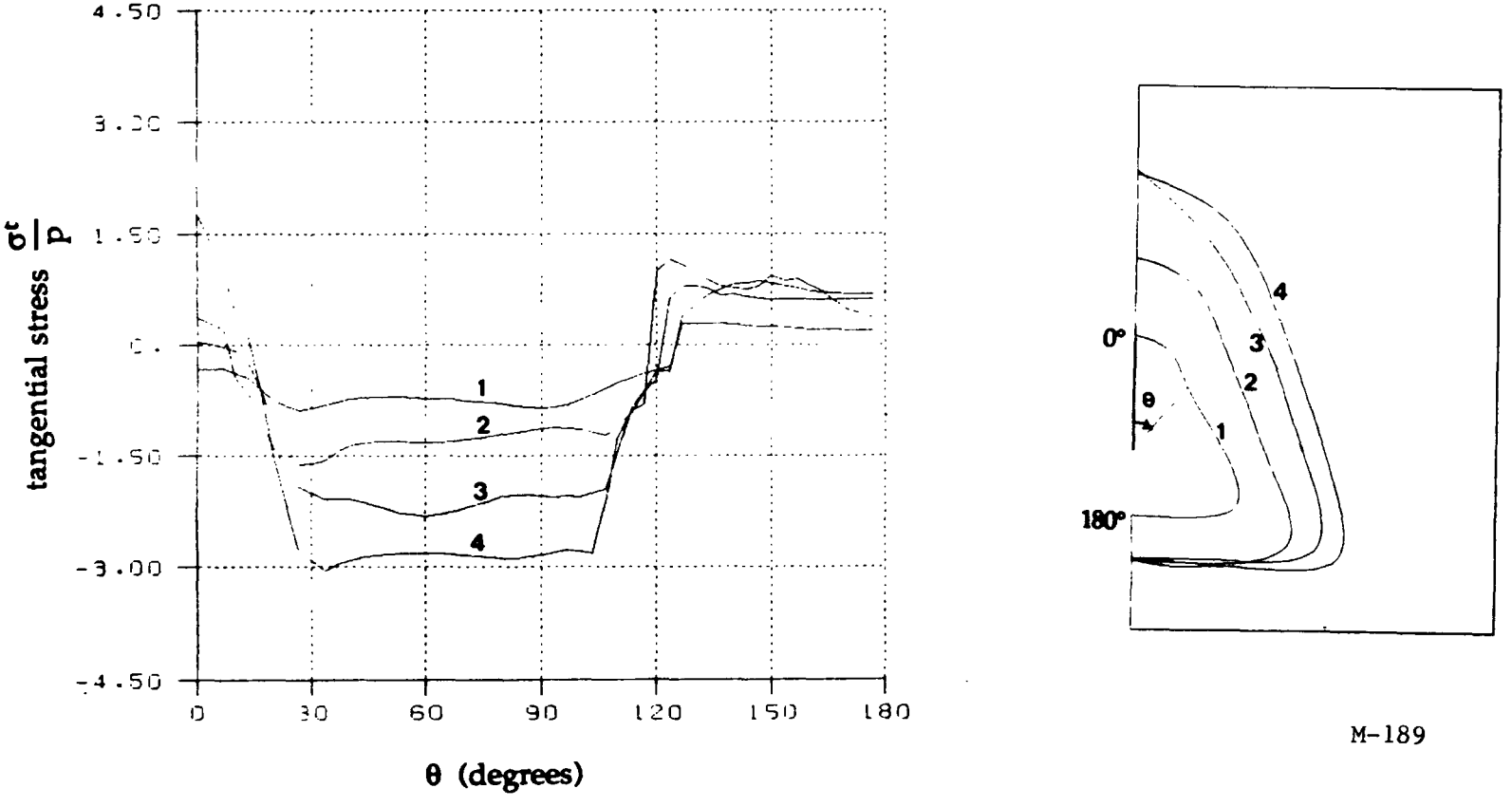

Fig. 12. Variation of the stress tangential to the hole boundary with angle θ for the numerical hole shapes of figs. 6(b) - 9(b).

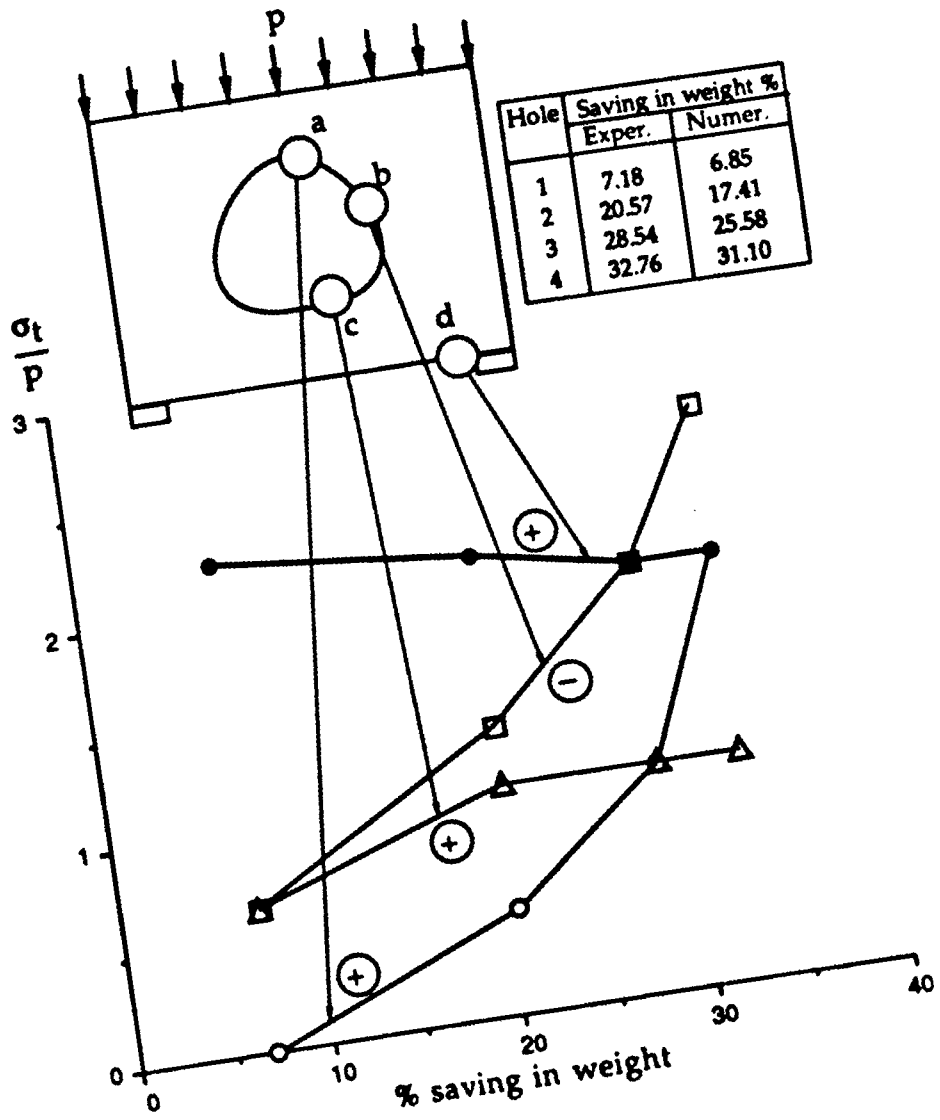

Hole	Saving in weight %	
	Exper.	Numer.
1	7.18	6.85
2	20.57	17.41
3	28.54	25.58
4	32.76	31.10

M-190

Fig. 13. Savings in weight corresponding to four steps of optimization and change in stresses at selected points.